Iranian Journal of Medical Physics

ijmp.mums.ac.ir

Investigation of LINAC Structural Effects on Photoneutron Specified Parameters Using FLUKA code

Mohammad Ashrafinia[1], Ashghar Hadadi[1*], Dariush Sardari[1], Elham Saeedzadeh[1]

1. Department of Medical Radiation Engineering, Science and Research Branch, Islamic Azad University, Tehran, Iran

ARTICLE INFO

Article type:
Original Article

Article history:
Received: Feb 14, 2019
Accepted: Apr 08, 2019

Keywords:
Fast Neutrons
Linac
Monte Carlo
FLUKA

ABSTRACT

Introduction: The utilization of high-energy photons in the medical linear accelerator can lead to photoneutron production. This study aimed to evaluate the effect of the physical components of the head, including flattening filter (FF) and multileaf collimator (MLC), as well as the dependence of therapeutic field size on the photoneutron spectrum, dose, and flux.

Material and Methods: The present study reported the simulation of the fundamental linac head components of the Varian Clinac 2100 performing in X-ray mode with 18 MV energy by the FLUKA code. The percentage depth dose and lateral dose profile were measured using a PTW thimble chamber to ensure the simulation reliability.

Results: Photoneutron spectrum analysis indicated that neutrons with highest relative biological effectiveness were delivered to the phantom surface, and opening the field from 0×0 to 40×40cm^2 shifted the spectrum by 24.545% to the higher energies. The target and the vicinity parts played the most prominent roles in neutron contamination. The relationship between the field size and the photoneutron dose was non-linear, and it reached a peak of 20×20 cm^2. Although using small fields formed by the MLC contribute to a lower dose compared to those shaped by the jaws, MLC-equipped machines result in 21.98% higher dose. Moreover, the flattening filter removal unexpectedly increased the isocenter photoneutron dose by 11.63%. This undesirable dose can be up to 2.54 mSv/Gy for the reference field at the isocenter while the out-of-field dose is about 0.5 mSv/Gy for most of the field dimensions.

Conclusion: As a result, it is critical to consider this unwanted absorbed dose, which is seriously influenced by the implemented therapeutic conditions.

►*Please cite this article as:*
Ashrafinia M, Hadadi A, Sardari D, Saeedzadeh E. Investigation of LINAC Structural Effects on Photoneutron Specified Parameters Using FLUKA code. Iran J Med Phys 2020; 17: 7-14. 10.22038/ijmp.2019.37678.1481.

Introduction

Photons and electrons are still common radiations used widely in linear accelerators (linacs), especially in underdeveloped countries. Although high-energy external beam radiotherapies are preferred for deeply-localized tumors, the utilization of such beams in linacs can lead to neutron contamination.

The interaction of high-energy photons (>7 MV) with some materials, especially nucleus with odd neutron number [1] and also the heavy ones produces photoneutron through (Y, n) [2-5] interaction and increases the energy leading to greater neutron yields [2, 3, 6-8]. Since electroneutral generation $(e, e'n)$ is not a significant phenomenon due to the much lower production cross section [2, 3, 9], the main focus of this study was to investigate photodisintegration interaction by the Monte Carlo (MC) simulation of the fundamental linac head components. The obtained results can make major contributions to photoneutron generation due to the high photo-nuclear cross sections [10].

Given the importance of neutron contamination, several studies have been performed to address the destructive effects of this issue. In this regard, some major problems of photoneutrons include the malfunctioning of the implemented electronic devices in radiotherapy rooms [11], disrupting the functionality of electronic implants [12, 13], creating errors in dosimetry in combined photon-neutron fields [14], producing the secondary active radioisotopes in the bunker, and delivering unexpected dose to the patients and the medical staff [3, 15]. Therefore, recent studies aimed to employ various methods to determine neutron flux and dose. Neutron-activation foils [3, 6, 8, 16], CR39 films [17, 18], bubble detector [2], Berthold Neutron Probe LB6411 [19], Polycarbonate track dosimeter [20], specific thermoluminescent dosimeters (TLDs) (e.g., TLD700H [21]), are among some of the devices utilized for the practical measurement. In most of these studies, the photoneutron dose was estimated indirectly using conversion factors [6, 18, 22, 23].

Given the neutral nature of neutrons and limitations in the practical measurements of neutrons, MC simulations (especially MCNP code) are valid methods for the evaluation of neutron contamination, which can provide precise results [5, 9, 10, 16, 19, 23-

Corresponding Author: Tel: +982144865179-82; E-mail: Haddadi14857@yahoo.com

26]. The FLUKA code system [27, 28] was not used widely in similar studies despite its strong capability to transport more than 60 particles. As a result, this study benefited from the utilization of FLUKA to simulate the detailed geometry implemented in the present model and also to speed up the process of obtaining results from numerous scoring cards used in the simulation [7, 14, 29, 30].

Different linac machines, such as Siemens Oncor [20, 31], ELEKTA Synergy Platform [2], Philips SL25 [2], Varian TrueBeam [19], Varian DHX [2], have been examined in neutron contamination investigations. This study was designed based on the implementation of Varian Clinac 2100C/D platform since it was acclaimed to have higher neutron yields compared to the devices with similar energies [5, 10, 16, 18, 24-26, 30, 32, 33].

The therapeutic conditions and physical parameters of linacs can highly affect neutron contamination. Treatment field size [2, 10, 17, 18, 23, 26, 29], photoneutron spectra [5, 15, 19], flattening filter (FF) free techniques [7, 30, 31], using multi-leaf collimators (MLCs) [2, 5, 16, 23, 24] in intensity modulated radiotherapy (IMRT) were previously studied; however, there is still controversy over the obtained results of previous. The purpose of this research was to investigate the influence of the physical head parameters on photoneutron flux, spectra, and dose distribution of the secondary neutrons.

Materials and Methods

Linac head simulation

The current study was a simulation of the fundamental linac head components of the Varian Clinac 2100 (Varian Medical Systems, Inc., USA) performing in X-ray mode with 18 MV energy using FLUKA code version 2011.2c-6-64bit, developed by Italian National Institute for Nuclear Physics (INFN) and European Organization for Nuclear Research (CERN). The major description of linac head components, including target, collimators, jaws, FF, ionization chamber, vacuum window, surround shields, and a Millenium 80-leaf MLC, were simulated based on the previously published data, manufacturer specification, and Varian confidential information. Moreover, considerable modifications in FF, jaws, and multileaf collimator (MLC) definition were carried out in line with these datasheets [18, 32, 33]. Figures 1, 2, and 3 show the three-dimensional view of the simulated head, FF, and MLC.

The mean kinetic energy of the incident beams, which are primary electrons on the target is 18.3 MeV [4, 5]. The investigations were based on Gaussian energy distribution regarding the definition of the primary electron (i.e., 3% of the mean energy with a 1 mm FWHM along with x and y components in the spatial distribution) [4, 5]. In addition, a 140×140 cm water phantom with the depth of 35 cm and large enough to calculate out-of-field dose [5] was considered for both photon and neutron dose estimation. The fundamental variables of the current research included flux, dose, and spectrum. Moreover, this study aimed to investigate the effect of the structural components of the head (including FF and MLC) and therapeutic field size on these variables.

To decline the statistical errors and reduce computation time, variance reduction techniques are commonly applied for simulation. In the current study, LAM-BIAS card was set in the FLUKA at 0.01 to reduce electron-photon interaction length and increase photon and neutron production gain. Moreover, the BIASING card was set to 10 to increase the importance of photon emission from the target. Furthermore, the energy cut-off of 7 MeV was considered for photon and electron transport in the simulation for all the components of the head except target, beryllium window, and water phantom.

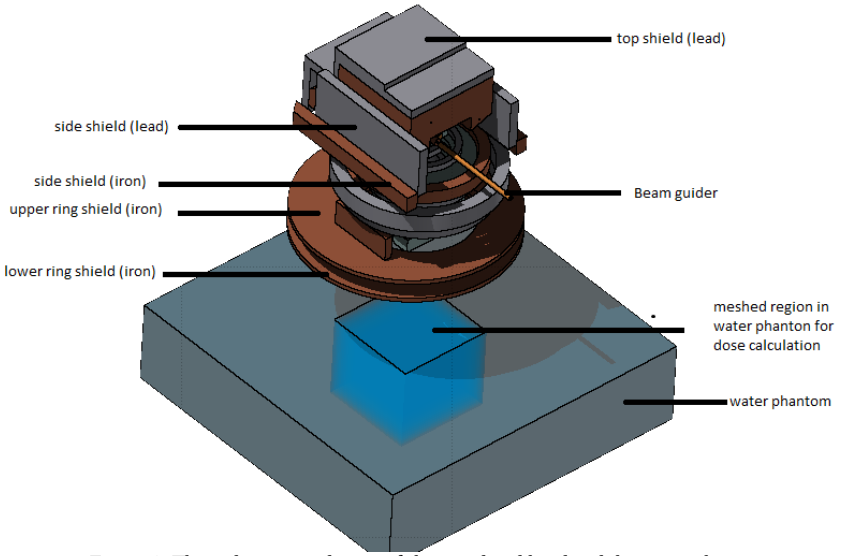

Figure 1. Three-dimensional view of the simulated head and the water phantom

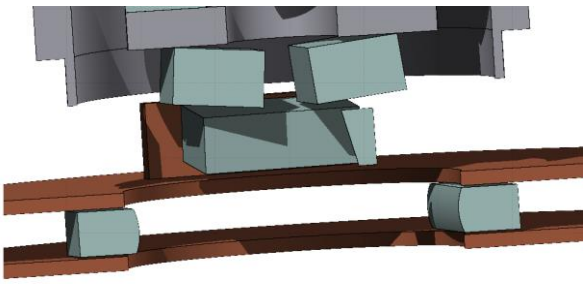

Figure 2. Simulated Y and X jaws, and retracted MLCs

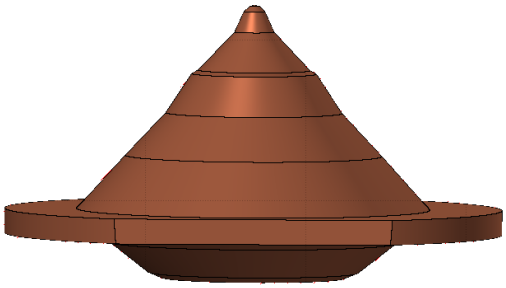

Figure 3. Detailed model of the Varian clinic 2100 flattening filter

Model Validation

To evaluate the validity of the simulation, in-plane dose profiles and percentage depth dose (PDD) curves of the MC estimation were compared with the experimental data. The MC calculation and practical measurement were both carried out under reference to clinical dosimetry conditions [34]. In addition, the 10×10 cm square field was formed by x and y jaws with entirely retracted MLCs, the gantry head angle was at 0 degree, and target to phantom surface distance (TSD), also called source to surface distance (SSD), of 100 cm was chosen to afford these conditions. The SSD=100 cm on the centerline was determined as the isocenter position. Furthermore, two meshes were created with 0.001 cm^3 voxel volume; one on the central axis of the head for PDD calculation and another at a 10-cm depth of the phantom along the in-plane direction to calculate the dose profile.

The experimental measurement of PDD and dose profile was performed using a PTW 31010 Semiflex thimble chamber detector (PTW dosimetry company, Freiburg, Germany) in the Varian Clinac 2100 machine at Imam Khomeini Hospital in Tehran, Iran, under reference conditions. Regarding the importance of photoneutrons in the present study, it was not possible to obtain PDD and dose profile for different field sizes due to the run-time limitations caused by the heavy geometry constructed in the present model.

Structural head component impact on photoneutrons

With regard to the constituents of the head, the participation ratio on photoneutron production was investigated using a mesh along the central axis from 50 cm above the target to 130 cm beneath it (i.e., the maximum depth of the phantom). The sizes of mesh cells constructed by the USRBIN card were 1×1×1 cmin all neutron calculations. The visualization of the photoneutrons flux and comparison with the therapeutic photons were carried out using a constructed two-dimensional mesh around the head to give a better understanding of the contamination distribution. Furthermore, FF and the MLC were individually removed from the simulation to examine the effect of these parts on photoneutron dose and flux.

Effect of treatment field size on photoneutron dose

This section of the study included various photon field sizes and their effects on the photoneutron dose equivalent. The square fields of 10×10, 20×20, 30×3, and 40×40 cm^2 were defined by the jaws with entirely retracted MLC. Furthermore, the smaller ones, including 1×1, 3×3, and 5×5 cm^2 usually used in IMRT, were determined by the MLCs. In MLC-shaped fields, jaws covered the fields partially and they were set to 1.2×1.2, 3.2 ×3.2, and 5.2×5.2 cm [5, 16, 24]. Furthermore, the entirely closed jaws and MLCs were used to define the 0×0 field.

In-field and out-of-field photoneutron dose were estimated using a 1 cm^3 voxels mesh created at the 1-cm depth of the phantom. The AMP74 was implemented in the input to activate the International Commission on Radiological Protection publication 74 (ICRP74) conversion coefficient [22] in the FLUKA. As a result, the neutron dose unit in the current study was in ambient dose equivalent (H^*[10]), and was also normalized to 1 Gy photon dost at d_{max} (the depth of the photon dose build-up) for the reference field using the method described by Bednarz [5].

Photoneutron spectra

This part of the study addressed the influence of the head components and also the depth of the water phantom on the photoneutron spectra. To this end, 20×20 cm^2 planar plates were designed and they were placed among the free spaces of the linac head's elements on the beamline as spectra scoring planes. These detectors consisted of 150 energy bins from thermal neutrons up to 19 MeV energy.

Results

MC Validation

Figures 4 and 5 illustrate the experimental and the theoretical PDD and dose profile of the Varian machine. The MC calculation of statistical errors in all points were less than 1%. The discrepancy between the measured and the calculated data in the shallow regions of the PDD down to the depth of 30 cm was less than 2.34%. Furthermore, the difference between the experimental measurement and the MC calculation of the dose profile in all points did not exceed 3.8%. Additionally, Table 1 provides the lists of other dosimetric parameters to ensure the validity of the current model.

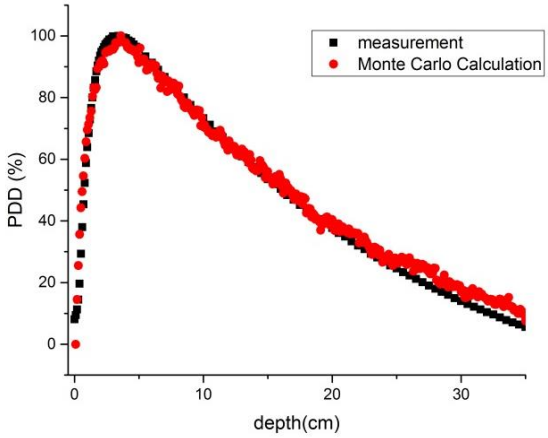

Figure 4. Calculated and measured percentage depth dose curves on the central axis of the head in the phantom

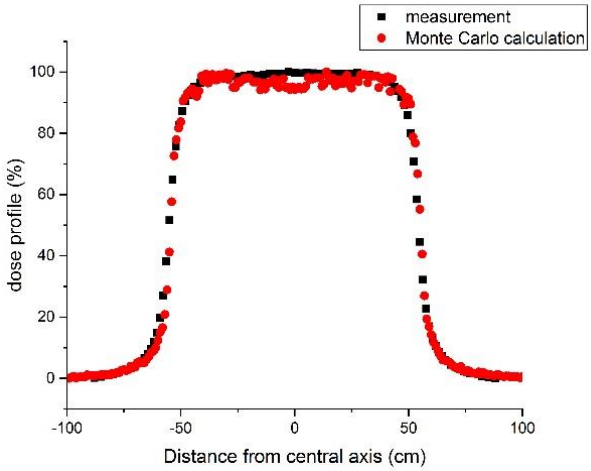

Figure 5. In-plane calculated and measured dose profile at the 10 cm depth of the phantom

Table 1. Dosimetric parameters of the Varian Clinac 2100 machine

Parameters	Practical measurement	MC calculation	BJR11 reference
Maximum photon dose depth (d_{max})	3.4 cm	3.6 cm	3.3 cm
Dose profile flatness	4.6%	3.4%	2.5%

Photoneutron flux distribution

Figure 6 shows the treatment beam flux for the standard field size, in which the slight radiation leakage of the head and some scatterings from the beam path can be observed. Figure 7 indicates the neutron contamination flux caused by the elements of the linac head. The comparison of these two figures (6 and 7) demonstrated that despite the beneficial role of the protective parts of the head in controlling the treatment beam toward the patient body, they were unable to shield the photoneutrons and rather intensified them. Moreover, as seen in Figure 7, water is the only barrier against photoneutrons due to the hydrogen atoms attendance.

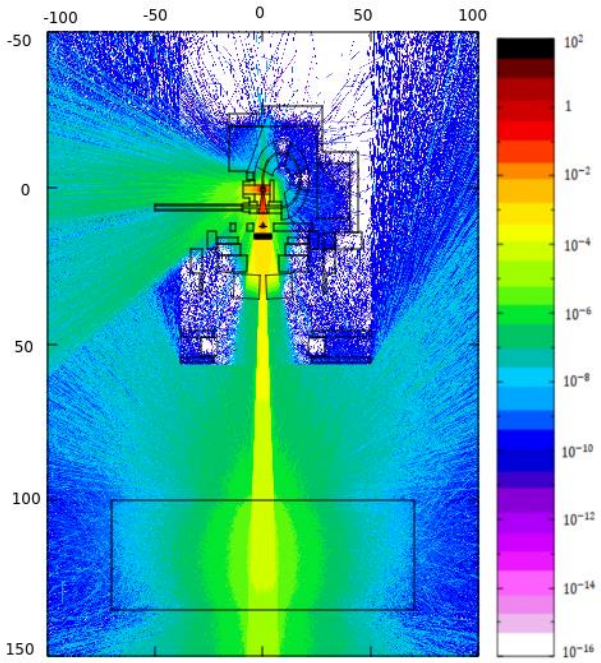

Figure 6. Therapeutic beam toward the water phantom for the $10\times10\ cm^2$ field

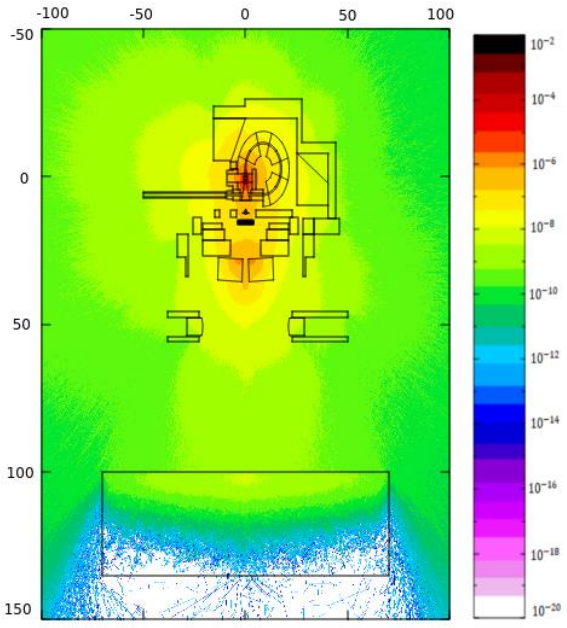

Figure 7. In-plane view of the neutron contamination distribution in Varian Clinac 2100 head

According to Figure 8 illustrating the photoneutrons total flux (i.e., thermal to fast) on the centerline, the target and the vicinity parts contributed the most to the neutron contamination. With the increase of the distance from the target, the exponential reduction of the fluence was observed in both directions on the axis. The elements located on the beamline, including FF and jaws, were made of heavy materials with a high photo-nuclear cross-

section, which enhanced the photoneutron flux. The associated peaks can be seen in Figure 8.

The FF contributed to photoneutron generation due to iron and tantalum ingredients, and its removal would eliminate the related peak and also decline the total flux by 31.2% at that point. As observed in Figure 8, although the elimination of the MLC-80 from the simulation has no visible impact on centerline flux increase due to their entire retraction, the decrease of 21.98% at isocenter dose occurred according to our calculations.

The Phantom-related peak in Figure 8 represents neutrons build-up at a 2-cm depth of the phantom and water has no significant role in photoneutron generation while photo-nuclear threshold energy in oxygen is about 16 MeV [10].

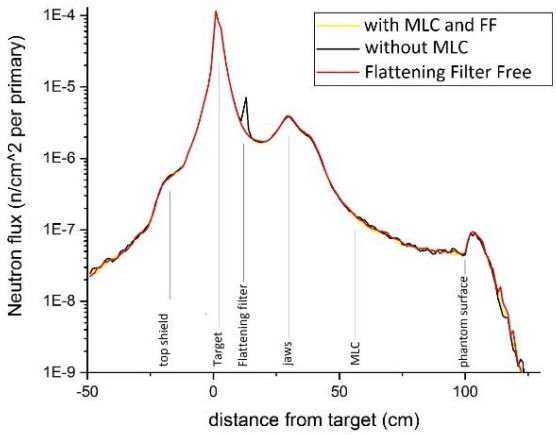

Figure 8. Influence of the components of the head on photoneutron flux along the central axis

Photoneutron dose changes with field size

Figure 9 shows the influence of field size on in-field and out-of-field dose. With the increase of the field size up to 20×20 cm^2, the photoneutron dose reached a top at the isocenter (more than 3.04 mSv/Gy) while opening the field further reduced the dose. The obtained results were in agreement with the findings of a study conducted by Brkic [31]. According to the current estimations, photoneutron dose exposure to the isocenter can be up to 2.54 mSv/Gy and more than 0.455 mSv/Gy at 70 cm of the centerline for the reference field. Table 2 summarizes the outcomes of the previously published articles.

photoneutron spectra

Figure 10 depicts the dependence of field size on the photoneutron spectrum. Changes in intensity distribution were negligible; however, 24.545% shift to the higher energies with opening the field from 0×0 to 20×20 cm^2 can be observed in the interval 100 KeV-1 MeV. The reason for this was the field openness, where the fast neutrons produced in the upper parts of the head, especially the target and the primary collimator, can easily reach the phantom surface without thermalization or absorption by the jaws and MLCs. Similarly, Brkic [31] reported similar findings for Siemens Oncor Machine.

Figure 11 presents the effect of the centerline components on the photoneutron spectrum. The increase of the distance from the target led to fast neutrons thermalization, particularly in low-lying parts of the elements of the head (collimators, jaws, and shields), resulting in thermal and epithermal intensity growth.

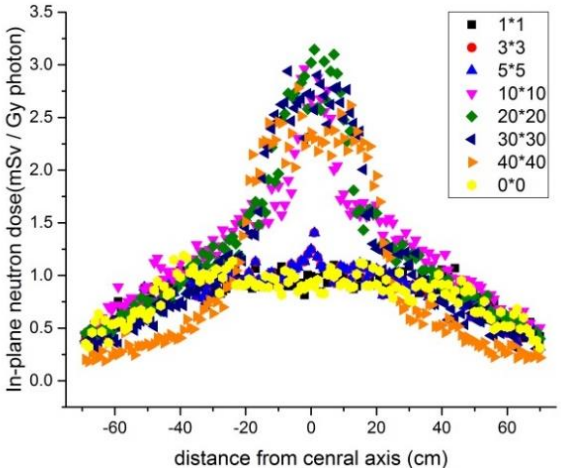

Figure 9. Photoneutrons dose profile changes with field sizes at a 1-cm depth of the phantom

Table 2. Photoneutron dose at the isocenter of the Varian Clinac 2100 for the reference field

Study	Dose (mSv/Gy)	Parameter
The current study	2.54	ambient dose equivalent (H^*_{10})
Howell [23]	2.34	ambient dose equivalent (H^*_{10})
Najem [7]	3.1	dose equivalent (H)
Alem-Bezoubiri [18]	3.5	ambient dose equivalent (H^*_{10})

Figure 12 shows the photoneutrons spectra taken from inside and outside the water phantom. An extreme point was visible between 100 keV and 1 MeV energies (black dots) that disappeared at the depth of 3 cm under the phantom surface (red dots). It demonstrated the highest radiation weighting factor for fast neutrons absorbed by the phantom superficial regions.

Discussion

The FF removal reduced the photoneutron total flux at the filter position (Figure 8). However, placing the FF on the beamline could also thermalize fast neutron production in the upper parts of the head. Its removal from the simulation could increase the fast neutrons flux at the isocenter resulting in 11.63% dose growth. These results were inconsistent with the obtained results from the studies conducted by Brkic [31] and Najem [7, 30] indicating that flattening filter free techniques would reduce the out-of-field photoneutron dose. The discrepancies obtained in this section may be due to the precise implemented filter simulation, different estimation position, or considering the filter along with all elements of the head.

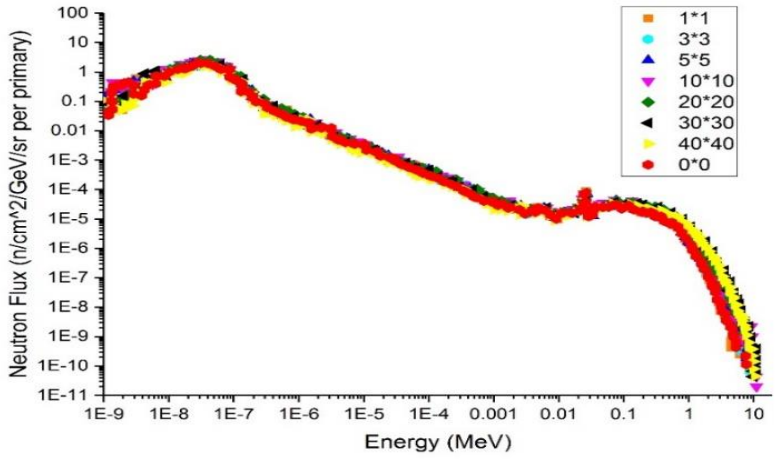

Figure 10. Changes in the photoneutron energy spectrum with opening the treatment field size

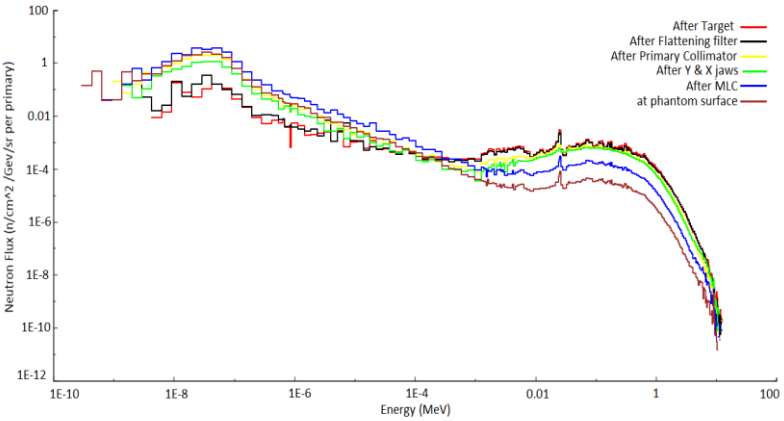

Figure 11. Effect of the components of the head on the photoneutron energy spectrum

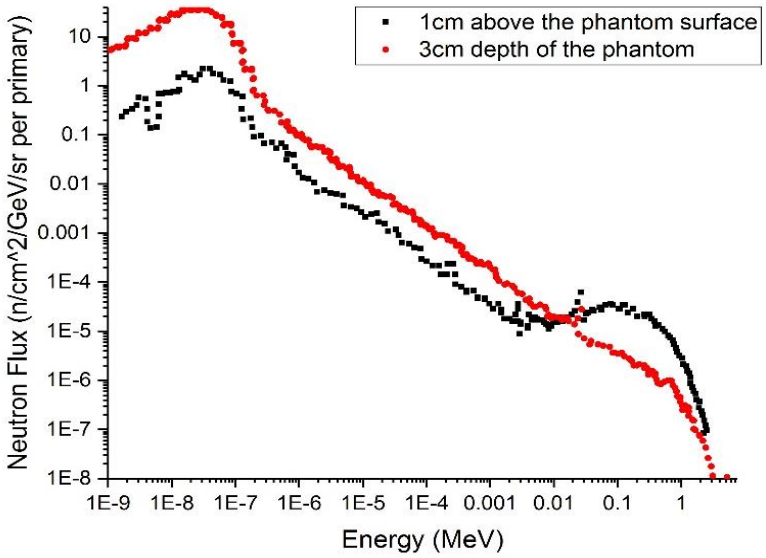

Figure 12. Photoneutron spectra at the surface and in a 3-cm depth of the phantom

As seen in Figure 9, MLC-shaped fields frequently used in IMRT modules contributed to a lower dose at the isocenter, compared to those formed by the Jaws. However, the findings of some studies indicated that IMRT delivered considerable photoneutron dose due to a longer beam-on-time and a higher number of monitor unit requirement [23]. Additionally, out-of-field photoneutron dose for most therapeutic field sizes was

about 0.5 mSv/Gy indicating that jaws, MLCs or other shielding elements cannot protect distally-located-organs against neutron contaminations. A complete prostate radiotherapy procedure almost always needs a total dose of more than 70 Gy depending on tumor histopathological characteristics, which deliver significant undesirable dose to these areas [35].

The increase of the distance from the target reduced the intensity of the fast neutrons (Figure 11). However, as shown in Figure 12, the patient's body still absorbed most of the fast neutrons with highest RBE emitted by the head (see also Figure 7). Consequently, the possibility of secondary skin cancer may significantly rise in these patients [36].

Since the majority of fast neutrons originated from the upper parts of the head (figures 7 and 8), scattering these fast neutron toward bunker space and interaction with shield wall materials may induce radionuclides with longer half-lives [15]. Although the patient's safety against neutron contaminations is our priority it should contain all structures of the linac head in the case of the secondary shield design.

Conclusion

The comparison of the implementation of MC codes in recent studies with FLUKA in the present study indicated that FLUKA can provide more reliable results. Additionally, its flair interface could suggest a feasible way of resolving the geometrical errors in the present model and also accelerated the process of obtained results. Based on the findings of the current study, the photoneutron dose varied remarkably in terms of field size and distance from the axis. This value can be beyond 2.54 mSv/Gy for jaw-shaped fields at the isocenter resulting in uncertainty in the prescribed dose of patients. Moreover, organs located outside the therapeutic field received an extremely noticeable dose from neutron contamination. This means there was not only the head protective elements defect in shielding the photoneutrons, but also intensified neutron production in these parts. Some previously published papers have found that implementing the flattening filter in conventional linear accelerators would partially increase the photoneutron absorbed dose. This is contrary to the results of this study, where flattening filter would absorb most of the fast neutrons which are responsible for high dose delivering. However, decisive conclusions need further studies. In conclusion, every single change in treatment setup significantly affects the quantity of the photoneutron dose delivering to the patient's body. Therefore, it is essential for empirical approaches to limit this undesired dose, especially in patient-specific treatment planning. Finally, it is suggested to propose a suitable secondary shield design as an immediate solution to reduce the photoneutron dose as much as possible, which is the subject of our next study.

Acknowledgment

The authors would like to show their gratitude to the medical physics department of the Tehran Imam Khomeini hospital for sharing their technical data on the Varian linac with us during the course of this research.

References

1. Chilton AB, Shultis JK, Faw RE. Principles of radiation shielding. 1984.
2. Biltekin F, Yeginer M, Ozyigit G. Investigating in-field and out-of-field neutron contamination in high-energy medical linear accelerators based on the treatment factors of field size, depth, beam modifiers, and beam type. Physica Medica. 2015 Jul 1;31(5):517-23.
3. Konefał A, Orlef A, Bieniasiewicz M. Measurements of neutron radiation and induced radioactivity for the new medical linear accelerator, the Varian TrueBeam. Radiation Measurements. 2016 Mar 1;86:8-15.
4. Sheikh-Bagheri D, Rogers DW. Monte Carlo calculation of nine megavoltage photon beam spectra using the BEAM code. Medical physics. 2002 Mar;29(3):391-402.
5. Bednarz B, Xu XG. Monte Carlo modeling of a 6 and 18 MV Varian Clinac medical accelerator for in-field and out-of-field dose calculations: development and validation. Physics in Medicine & Biology. 2009 Jan 14;54(4):N43.
6. Yücel H, Çobanbaş İ, Kolbaşı A, Yüksel AÖ, Kaya V. Measurement of photo-neutron dose from an 18-MV medical linac using a foil activation method in view of radiation protection of patients. Nuclear Engineering and Technology. 2016 Apr 1;48(2):525-32.
7. Najem MA, Abolaban FA, Podolyák Z, Spyrou NM. Neutron production from flattening filter free high energy medical linac: A Monte Carlo study. Radiation Physics and Chemistry. 2015 Nov 1;116:176-80.
8. Cardenas CE, Nitsch PL, Kudchadker RJ, Howell RM, Kry SF. Out-of-field doses and neutron dose equivalents for electron beams from modern Varian and Elekta linear accelerators. Journal of applied clinical medical physics. 2016 Jul;17(4):442-55.
9. Yani S, Tursinah R, Rhani MF, Soh RC, Haryanto F, Arif I. Neutron contamination of Varian Clinac iX 10 MV photon beam using Monte Carlo simulation. InJournal of Physics: Conference Series 2016 Mar (Vol. 694, No. 1, p. 012020). IOP Publishing.
10. Ma A, Awotwi-Pratt J, Alghamdi A, Alfuraih A, Spyrou N. Monte Carlo study of photoneutron production in the Varian Clinac 2100C linac. Journal of Radioanalytical and Nuclear Chemistry. 2007 Nov 24;276(1):119-23.
11. Kry SF, Johnson JL, White RA, Howell RM, Kudchadker RJ, Gillin MT. Neutron-induced electronic failures around a high-energy linear accelerator. Medical physics. 2011 Jan;38(1):34-9.
12. Zecchin M, Morea G, Severgnini M, Sergi E, Baratto Roldan A, Bianco E, et al. Malfunction of cardiac devices after radiotherapy without direct exposure to ionizing radiation: mechanisms and experimental data. Ep Europace. 2015 Sep 1;18(2):288-93.
13. Marbach JR, Sontag MR, Van Dyk J, Wolbarst AB. Management of radiation oncology patients with

implanted cardiac pacemakers: Report of AAPM Task Group No. 34. Medical physics. 1994 Jan;21(1):85-90.
14. Horst F, Czarnecki D, Zink K. The influence of neutron contamination on dosimetry in external photon beam radiotherapy. Medical physics. 2015 Nov;42(11):6529-36.
15. Juste B, Morató S, Miró R, Verdú G, Díez S. MCNP6 unstructured mesh application to estimate the photoneutron distribution and induced activity inside a linac bunker. Radiation Physics and Chemistry. 2017 Aug 1;137:18-22.
16. Kry SF, Titt U, Followill D, Pönisch F, Vassiliev ON, White RA, et al. A Monte Carlo model for out-of-field dose calculation from high-energy photon therapy. Medical physics. 2007 Sep;34(9):3489-99.
17. Jahangiri M, Hejazi P, Hashemi SM, Haghparast A, Hajizadeh B. The effect of field size and distance from the field center on neutron contamination in medical linear accelerator. International Journal of Advanced Biological and Biomedical Research (IJABBR). 2015 Jan 1;3(1):97-104.
18. Alem-Bezoubiri A, Bezoubiri F, adreddine A, Mazrou H, Lounis-Mokrani Z. Monte Carlo estimation of photoneutrons spectra and dose equivalent around an 18 MV medical linear accelerator. Radiation Physics and Chemistry. 2014 Apr 1;97:381-92.
19. Sumini M, Isolan L, Cucchi G, Sghedoni R, Iori M. A Monte Carlo model for photoneutron generation by a medical LINAC. Radiation Physics and Chemistry. 2017 Nov 1;140:345-8.
20. Hakimi A, Sohrabi M, Rabie Mahdavi S. Effects of field size and depth on photoneutron dose equivalent distributions in an 18 MV X-ray medical accelerator. Radiation protection dosimetry. 2017 Mar 1;176(4):354-64.
21. Nedaie HA, Darestani H, Banaee N, Shagholi N, Mohammadi K, Shahvar A, et al. Neutron dose measurements of Varian and Elekta linacs by TLD600 and TLD700 dosimeters and comparison with MCNP calculations. Journal of medical physics/Association of Medical Physicists of India. 2014 Jan;39(1):10.
22. ICRP Publication 74. Conversion Coefficients for use in Radiological Protection against External Radiation. 1997.
23. Howell RM, Ferenci MS, Hertel NE, Fullerton GD. Investigation of secondary neutron dose for dynamic MLC IMRT delivery. Medical physics. 2005 Mar;32(3):786-93.
24. Kry SF, Titt U, Pönisch F, Followill D, Vassiliev ON, Allen White R, et al. A Monte Carlo model for calculating out-of-field dose from a Varian beam. Medical physics. 2006 Nov;33(11):4405-13.
25. Vega-Carrillo HR, Martinez-Ovalle SA, Lallena AM, Mercado GA, Benites-Rengifo JL. Neutron and photon spectra in LINACs. Applied Radiation and Isotopes. 2012 Dec 1;71:75-80.
26. Ezzati A, Studenski M. Neutron dose in and out of 18MV photon fields. Applied Radiation and Isotopes. 2017; 122: 186-92.
27. Böhlen TT, Cerutti F, Chin MP, Fassò A, Ferrari A, Ortega PG, et al. The FLUKA code: developments and challenges for high energy and medical applications. Nuclear data sheets. 2014 Jun 1;120:211-4.
28. Ferrari A, Sala PR, Fasso A, Ranft J. FLUKA: A multi-particle transport code (Program version 2005). 2005.
29. Patil BJ, Chavan ST, Pethe SN, Krishnan R, Bhoraskar VN, Dhole SD. Estimation of neutron production from accelerator head assembly of 15 MV medical LINAC using FLUKA simulations. Nuclear Instruments and Methods in Physics Research Section B: Beam Interactions with Materials and Atoms. 2011 Dec 15;269(24):3261-5.
30. Najem MA, Spyrou NM, Podolyák Z, Abolaban FA. The physical characteristics of the 15 MV Varian Clinac 2100C unflattened beam. Radiation Physics and Chemistry. 2014 Feb 1;95:205-9.
31. Brkić H, Ivković A, Kasabašić M, Sovilj MP, Jurković S, Štimac D, et al. The influence of field size and off-axis distance on photoneutron spectra of the 18 MV Siemens Oncor linear accelerator beam. Radiation Measurements. 2016 Oct 1;93:28-34.
32. Martinez-Ovalle SA, Barquero R, Gomez-Ros JM, Lallena AM. Neutron dose equivalent and neutron spectra in tissue for clinical linacs operating at 15, 18 and 20 MV. Radiation protection dosimetry. 2011 Jan 12;147(4):498-511.
33. Mao XS, Kase KR, Johnsen S, Liu JC, Nelson WR, Kleck JH. Neutron sources in the Varian Clinac 2100C/2300C medical accelerator calculated by the EGS4 code. Health Phys.. 1996;72(SLAC-PUB-7077):524-9.
34. Almond PR, Biggs PJ, Coursey BM, Hanson WF, Huq MS, Nath R, et al. AAPM's TG-51 protocol for clinical reference dosimetry of high-energy photon and electron beams. Medical physics. 1999 Sep 1;26(9):1847-70.
35. Bezak E, Takam R, Marcu LG. Peripheral photon and neutron doses from prostate cancer external beam irradiation. Radiation protection dosimetry. 2015 Jan 5;167(4):591-601.
36. Expósito MR, Sánchez-Nieto B, Terrón JA, Domingo C, Gómez F, Sánchez-Doblado F. Neutron contamination in radiotherapy: Estimation of second cancers based on measurements in 1377 patients. Radiotherapy and Oncology. 2013 May 1;107(2):234-41.